Available online at www.sciencedirect.com
SCIENCE DIRECT®
Journal of Power Sources 141 (2005) 193–197
JOURNAL OF POWER SOURCES
www.elsevier.com/locate/jpowsour

Deterioration mechanism of nickel metal-hydride batteries for hybrid electric vehicles

Katsuhiko Shinyama*, Yoshifumi Magari, Kiyoshi Kumagae, Hiroshi Nakamura, Toshiyuki Nohma, Masao Takee, Koji Ishiwa

Mobile Energy Company, Sanyo Electric Co., Ltd., 7-3-2 Ibukidai-higashimachi, Nishi-ku, Kobe, Hyogo 651-2242, Japan

Received 28 July 2004; received in revised form 3 September 2004; accepted 3 September 2004
Available online 26 November 2004

Abstract

The deterioration mechanism of nickel metal-hybrid batteries for hybrid electric vehicles (HEVs) has been investigated. For HEV use, the deterioration of the batteries is caused by the degradation of the positive electrode which is influenced by the migration of the constituent elements of the negative electrode alloy as well as by the oxidation of the negative electrode. Based on the elucidated deterioration mechanism, the degradation of the positive electrode has been suppressed by employing a hydrogen-absorbing alloy with higher oxidation resistibility for the negative electrode, prolonging the cycle life of nickel metal-hydride batteries for HEVs.

Keywords: Nickel metal-hydride battery; Hybrid electric vehicle; Deterioration mechanism

1. Introduction

Recently, hybrid electric vehicles (HEVs) have been receiving much attention from both environmental and economical points of view and the development of HEVs has accordingly been getting intensive [1]. One of the most important components of HEVs is a rechargeable battery used for powering and regenerating. Almost all the commercialized HEVs employ nickel metal-hydride batteries because of their better combination of output power, capacity, life, reliability and cost [2–6]. For the nickel metal-hydride batteries for HEVs, high output power in a wide range of temperatures is strongly required as it is directly related to the driving performance and fuel consumption of HEVs in various circumstances [7]. In addition, the high output power must be maintained for a longer period than in consumer uses. For example, California Air Resources Board (CARB) which is a governing authority influential to car manufacturers requires a long battery life of 15 years or 150,000 miles to partial zero emission vehicle (PZEV).

In order to achieve such long battery life, it is very important to improve both the negative and positive electrodes based on the deterioration mechanism of the nickel metal-hydride batteries in HEV usage. For batteries for consumer uses, it is known that the decrease of the electrolyte in the separator is a dominant factor of the deterioration. Thus, suppressing the oxidation of the hydrogen-absorbing alloy for the negative electrode which consumes the electrolyte in the cell is important [8–12]. Suppressing the release of the electrolyte together with the inner gas from the cell is also important for this purpose. The oxidation of the alloy and the release of the electrolyte are related to the oxygen evolution near fully charged state. On the contrary, batteries for HEVs are rarely fully charged or discharged but are normally used at a medium state of charge, where they are repeatedly charged and discharged in a pulse-like pattern at higher current than in consumer uses. In addition, batteries for HEVs are often used at a higher temperature than in consumer uses. The deterioration mechanism of batteries for HEVs may thus be different

* Corresponding author. Tel.: +81 78 993 1129; fax: +81 78 993 1094.
E-mail address: sinyama@sm.energy.sanyo.co.jp (K. Shinyama).

0378-7753/$ – see front matter © 2004 Elsevier B.V. All rights reserved.
doi:10.1016/j.jpowsour.2004.09.010

from that for other uses since the charge–discharge pattern is quite different. However, few reports have been made on this issue. In this study, we report the deterioration mechanism of batteries for HEVs and the improvement for longer battery life based on the elucidated deterioration mechanism.

2. Experimental

Cylindrical sealed-type D-size cells (32.3 mm in diameter and 58.5 mm in height) with nominal capacity of 6.5 Ah were prepared. A sintered nickel positive electrode comprised nickel hydroxide coprecipitated with cobalt and zinc. A pasted hydrogen-absorbing alloy negative electrode comprised $MmNi_{3.6}Co_{0.4}Al_{0.3}Mn_{0.5}$ (Mm: misch metal) alloy. Both the electrodes were wound with a hydrophilic treated polyolefin separator. The electrolyte was composed of potassium hydroxide, sodium hydroxide and lithium hydroxide and its concentration was 7N.

Life tests were conducted under following two conditions accelerated by temperature:

(A) simulating an actual HEV driving pattern at 45 °C;
(B) 50 A pulse charge–discharge, state of charge (SOC) 40–60% at 45 °C.

The output power was measured as follows. After being charged to SOC 50%, a test cell was discharged for 10 s at various currents at 25 °C and the maximum discharge current was calculated when the battery voltage reached 0.9 V. In order to investigate the deterioration of the positive and negative electrodes, the DC-resistances of both the electrodes after cycling were also measured by inserting an Hg/HgO reference electrode into the cell.

The composition of the positive and negative electrodes was analyzed using ICP. The positive electrode was further investigated using SEM, EPMA and XRD. The surface area of the positive electrode was measured using BET method.

In order to evaluate the effect of the resolved elements from the negative electrode on the output power of the positive electrode, a three electrode test cell with a working electrode of nickel hydroxide, a counter electrode of hydrogen-absorbing alloy and a reference electrode of Hg/HgO was used.

3. Results and discussion

3.1. Cycle characteristics of the batteries simulating an actual HEV driving pattern

The change in the output power during HEV driving pattern cycling is shown in Fig. 1. Under this accelerated condition at 45 °C, the maximum discharge current decreased down to 73% of the initial value at 90 kmiles as the corresponding distance increased.

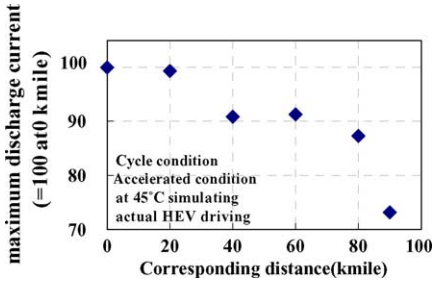

Fig. 1. Change in the output power during HEV driving pattern cycling.

The change in DC-resistance of the cell and the positive and negative electrodes before and after cycling is shown in Table 1. The cell DC-resistance increased by 0.65 mΩ from 2.12 mΩ at 0 kmiles to 2.77 mΩ at 90 kmiles. The corresponding increase in the resistance can be separated into 0.41 mΩ for the positive electrode and 0.24 mΩ for the negative electrode. Thus, it is found that the positive electrode gives a larger contribution to the total increase in the resistance than the negative electrode even when a sintered positive electrode which has been considered to be more durable than a non-sintered positive electrode is used.

Table 2 shows the change in the composition of the negative electrode alloy. The all values are normalized by the respective initial values. The oxygen content increased linearly with respect to the corresponding distance, more than 2.5 times larger compared to the initial value. The degradation of the negative electrode is considered to be due to the surface oxidation of the hydrogen-absorbing alloy. The aluminum and manganese contents of the alloy decreased by 16% compared to the initial values resulting from the oxidation and dissolution, whereas there was little change for the other constituent elements.

The change in the composition of the positive electrode is shown in Table 3. All values are normalized by the respective initial values. Aluminum and manganese, both of which were not contained originally in the positive electrode, were

Table 1
DC-resistance of the cell and the positive and negative electrodes before and after cycling

Corresponding distance (kmiles)	0	90
Cell resistance (mΩ)	2.12	2.77
Positive electrode resistance (mΩ)	1.58	1.98
Negative electrode resistance (mΩ)	0.55	0.79

Table 2
The amount of nickel, cobalt, aluminum, manganese, lanthanum and oxygen in the negative electrode alloy at 90 kmiles

Element	Amount
Ni	104
Co	103
Al	84
Mn	84
La	97
O	257

All values were normalized at 0 kmiles.

Table 3
The amount of nickel, cobalt, zinc, aluminum and manganese in the positive electrode alloy at 90 kmiles

Element	Amount
Ni	106
Co	91
Zn	87
Al	250
Mn	111

All values were normalized at 0 kmiles.

observed after cycling. In particular, the amount of aluminum increased by 250% at 90 kmiles. The cross-sectional microscopic images of the positive electrode at 90 kmiles are shown in Fig. 2. The white part of the SEM image is the current collector and the gray part is the nickel hydroxide active material. Aluminum and manganese detected with the chemical analysis were observed in the positive electrode as shown in the EPMA images. Aluminum was observed throughout the electrode and manganese was observed on the surface of the electrode.

Change in the crystal structure of the discharged positive electrodes after cycling was examined using XRD. There is a peak observed near 11.5° assigned to α-type $Ni(OH)_2$ at 90 kmiles as shown in Fig. 3. This result indicates the formation of γ-type NiOOH since α-type $Ni(OH)_2$ is known as a discharge product of γ-type NiOOH. At initial stage the charge and discharge reactions occur between β-type $Ni(OH)_2$ and β-type NiOOH [13,14]. At 90 kmiles, however, part of the charge and discharge reactions occur between α-type $Ni(OH)_2$ and γ-type NiOOH. This γ-type NiOOH is reported to be less reactive than β-type NiOOH [15].

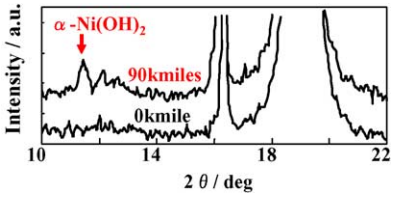

Fig. 3. XRD profiles of positive electrodes before and after cycling.

Table 4
Specific surface area of the positive electrodes before and after cycling

Corresponding distance (kmiles)	0	90
Specific surface area ($m^2\ g^{-1}$)	21.6	18.2

The cross-sectional SEM images of the positive electrodes before and after cycling are shown in Fig. 4. The size of the active material particles is several tens of nm. A morphological change was observed in the positive electrode materials: its initial needle-like and stereoscopic shape changed to a rounded and flat shape after degradation. The specific surface area measured using BET method correspondingly decreased from 21.6 to 18.2 $m^2\ g^{-1}$ as shown in Table 4. These observations above suggest that the dissolution of aluminum and/or manganese from the negative electrode alloy promotes the formation of less reactive γ-type NiOOH and the decrease in the surface of the positive electrode materials, leading to the increase in the resistance of the positive electrode.

3.2. *Verification of the deterioration mechanisms of the positive electrode*

The effect of aluminum and manganese on the characteristics of the positive electrode was examined using a three

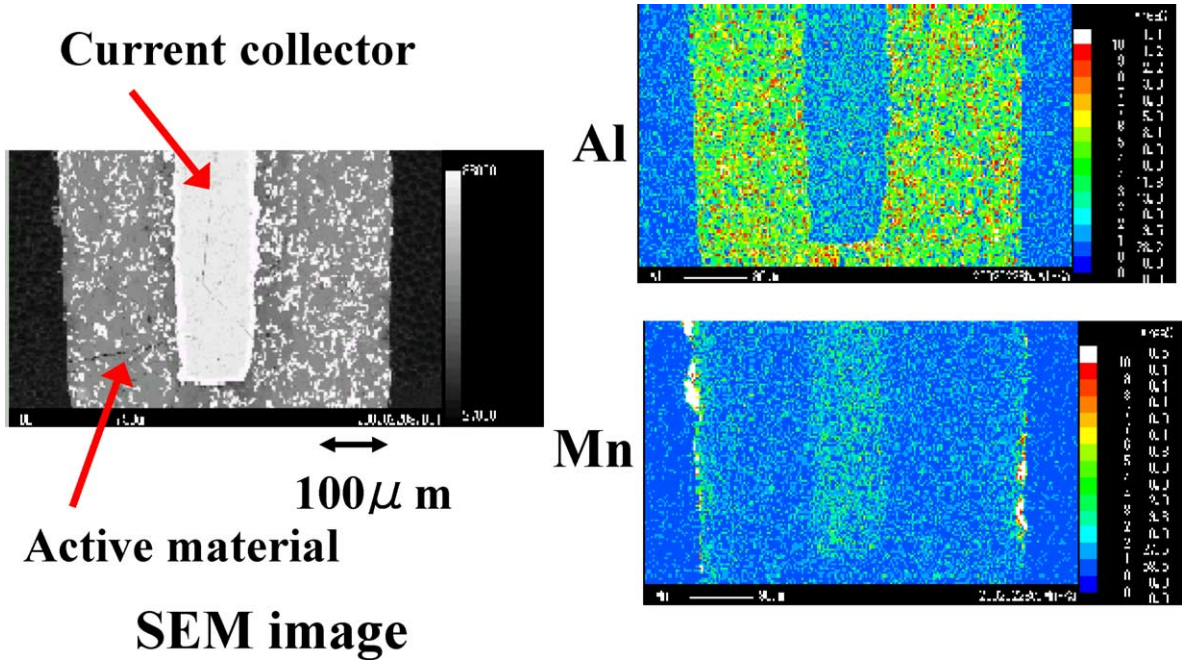

Fig. 2. Cross-section images of the positive electrode after 90 kmiles.

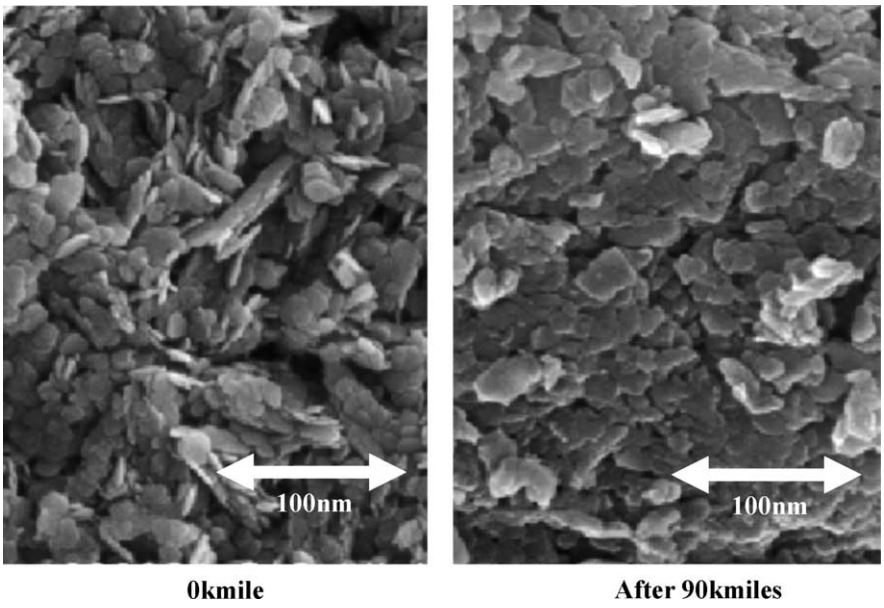

Fig. 4. Cross-sectional SEM images of the positive electrode before and after cycling.

electrode test cell. More specifically, manganese metal or aluminum hydroxide was excessively added into the electrolyte and a partial charge–discharge cycle test from SOC 40 to 60% was conducted up to 1000 cycles for each additive. The effect of aluminum and manganese on the positive electrode resistance and the specific surface area is shown in Table 5. The addition of aluminum brought an increase in the resistance by 14 mΩ which corresponded to 6% of the initial resistance, compared to the electrode without additive. The addition of aluminum also decreased the specific surface area by 2.0 $m^2\,g^{-1}$ compared to the electrode without additive. This result indicates that the dissolution of the aluminum in the negative electrode into the electrolyte and migration to the positive electrode promotes both the increase in the resistance and decrease in the surface area of the positive electrode. On the contrary, the addition of manganese brought neither an increase in the DC-resistance nor a decrease in the surface area.

No peaks assigned to γ-type NiOOH or α-type $Ni(OH)_2$ were detected in the XRD pattern in spite of the increase in the resistance of the positive electrode. This is considered to be because the increase in the resistance of the positive electrode by 6% was not large enough for γ-type NiOOH to be detected compared to the increase by 25% for the previous detection of the α-type $Ni(OH)_2$ in Fig. 3.

Table 5
Effect of Al and Mn on the positive electrode resistance and the specific surface area

	Added element	
	Al	Mn
DC-resistance at 1000 cycles (change from the electrode without additive) (mΩ)	+14	±0
Specific surface area ($m^2\,g^{-1}$)	−2.0	+0.1

3.3. Improvement of cycle life based on the deterioration mechanism

Based on the results discussed above, it is found that the improvement of the corrosion resistibility of the negative electrode alloy is essential for suppressing the deterioration of the nickel metal-hydride batteries for HEVs. In practice, the corrosion resistibility of the negative electrode alloy has been improved by optimizing the alloy composition and the alloy production conditions such as annealing condition. More specifically on the alloy composition the amount of cobalt and aluminum both of which are known to suppress the pulverization and oxidation of the alloy particles and the stoichiometry of the alloy have been increased. It is noted that the amount of aluminum has been increased in order to suppress the dissolution of aluminum into the electrolyte. Cycle performance of a cell using the improved negative electrode alloy is shown in Fig. 5. The test was a 50 A pulse charge–discharge life test accelerated by temperature at 45 °C. The cycle life has been prolonged by using the improved alloy: the maximum discharge current maintained

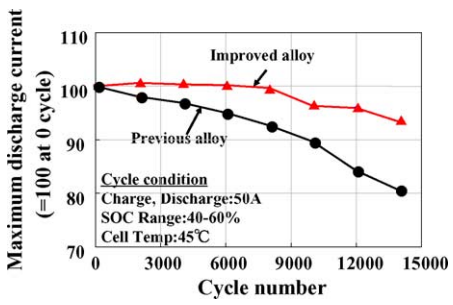

Fig. 5. Improvement of cycle characteristics using a hydrogen-absorbing alloy with higher oxidation resistibility.

Table 6
Oxygen content in the negative electrode and positive electrode resistance at 14,000 cycles using a hydrogen-absorbing alloy with higher oxidation resistibility

Negative electrode	Improved alloy	Previous alloy
Oxygen content (wt.%)	1.48	2.72
Positive electrode resistance (mΩ)	1.42	1.88

94% of the initial value at 14,000 cycles compared to 80% for the previous alloy.

Table 6 shows the oxygen content of the negative electrode alloy and the positive electrode resistance after the cycle test. The oxygen content was reduced by 46% from 2.72 to 1.48 wt.% and the positive electrode resistance was accordingly reduced by 24% from 1.88 to 1.42 mΩ by using the improved alloy instead of the previous alloy.

4. Conclusion

The deterioration mechanism of output power of nickel metal-hydride batteries for HEVs has been investigated. The output power declining during cycling is due mainly to the increase of the positive electrode resistance and partly to that of the negative electrode resistance. The increase in the negative electrode resistance is caused by the surface oxidation of the hydrogen-absorbing alloy. The increase in the positive electrode resistance is promoted by the migration of aluminum from the negative electrode to the positive electrode. Cycle performance of the D-cell for HEVs has been largely improved by suppressing the oxidation of the negative electrode alloy and the dissolution of its constituent elements by using a hydrogen-absorbing alloy with higher oxidation resistibility.

References

[1] O. Bitsche, G. Gutmann, J. Power Sources 127 (2004) 8.
[2] I. Yonezu, Proceedings of the Second International Advanced Automotive Battery Conference, 2002, p. 26.
[3] M. Verbrugge, E. Tate, J. Power Sources 126 (2004) 236.
[4] Y.-F. Yang, J. Power Sources 75 (1998) 19.
[5] A. Taniguchi, N. Fujioka, M. Ikoma, A. Ohta, J. Power Sources 100 (2001) 117.
[6] P. Gofford, J. Adams, D. Corrigan, S. Venkatesan, J. Power Sources 80 (1999) 157.
[7] S. Yuasa, N. Fujioka, K. Kanamaru, O. Takahashi, Proceedings of the 18th International Electric Vehicle Symposium, 2001, p. 52.
[8] O. Arnaud, P. Barbic, P. Bernard, A. Bouvier, B. Knosp, B. Riegel, M. Wohlfahrt-Mehrens, J. Alloy Compd. 330–332 (2002) 262.
[9] T. Sakai, H. Ishikawa, K. Oguro, C. Iwakura, H. Yoneyama, J. Electrochem. Soc. 134 (1987) 558.
[10] T. Sakai, H. Miyamura, N. Kuriyama, A. Kato, K. Oguro, H. Ishikawa, J. Electrochem. Soc. 137 (1990) 795.
[11] Z. Zhou, J. Yan, Y. Li, D. Song, Y. Zhang, J. Power Sources 72 (1998) 236.
[12] T. Sakai, K. Oguro, H. Miyamura, N. Kuriyama, A. Kato, H. Ishikawa, C. Iwakura, J. Less-Common Met. 161 (1990) 193.
[13] H. Bode, K. Dehmelt, J. Witte, Electrochim. Acta 11 (1966) 1079.
[14] R. Barnard, C.F. Randell, F.Y. Tye, J. Appl. Electrochem. 10 (1980) 109.
[15] S. Takeuchi, S. Magaino, K. Kobayakawa, Y. Sato, Electrochemistry 68 (2000) 977.